Journal of Solid State Chemistry **163,** 37–43 (2002)
doi:10.1006/jssc.2001.9350, available online at http://www.idealibrary.com on IDEAL®

$EuZn_2Si_2$ and $EuZn_2Ge_2$ Grown from Zn or Ga(In)/Zn Flux

A. Grytsiv,*[,1] D. Kaczorowski,† A. Leithe-Jasper,*[,2] P. Rogl,*[,1,3] C. Godart,‡ M. Potel,§ and H. Noël§

*Institut für Physikalische Chemie, Universität Wien, Währingerstr. 42, A-1090 Wien, Austria; †W. Trzebiatowski Institute for Low Temperature and Structure Research, Polish Academy of Sciences, P.O. Box 1410, P-50-950 Wroclaw, Poland, ‡CNRS-UPR209, ISCSA, 2-8 rue Henri Dunant, F94320 Thiais, France and LURE, CNRS, Universite Paris Sud, 91405 Orsay, France; and §Laboratoire de Chimie du Solide et Inorganique Moléculaire, UMR CNRS 6511, Université de Rennes I, Avenue du Général Leclerc, F-35042 Rennes Cedex, France

Received April 5, 2001; in revised form July 2, 2001; accepted August 9, 2001; published online November 27, 2001

Single crystals of the novel ternary compounds $EuZn_2Si_2$ and $EuZn_2Ge_2$ were grown from pure gallium, indium, or zinc metal used as a flux solvent. Crystal properties were characterized using X-ray single-crystal analyses via Gandolfi and Weissenberg film techniques and by four-circle X-ray single-crystal diffractometry. The new compounds crystallize with ternary derivative structures of $BaAl_4$, i.e., $EuZn_2Si_2$ with $ThCr_2Si_2$-type ($a = 0.42607(2)$ nm, $c = 1.03956(5)$ nm, $I4/mmm$, $R_1 = 0.038$) and $EuZn_2Ge_2$ with $CaBe_2Ge_2$-type ($a = 0.43095(2)$ nm, $c = 1.07926(6)$ nm, $P4/nmm$, $R_1 = 0.067$). XAS and magnetic measurements on $EuZn_2Si_2$ and $EuZn_2Ge_2$ revealed in both compounds the presence of Eu^{2+} ions carrying large magnetic moments, which order magnetically at low temperatures. The magnetic phase transition occurs at $T_N = 16$ and 7.5 K for the silicide and the germanide, respectively. In $EuZn_2Si_2$ there occurs a spin reorientation at 13 K and furthermore some canting of antiferromagnetically ordered moments below about 10 K. In $EuZn_2Ge_2$ a canted antiferromagnetic structure is formed just at T_N. © 2002 Elsevier Science

Key Words: **europium compounds; X-ray single-crystal refinement; $EuZn_2Si_2$ with $ThCr_2Si_2$-type; $EuZn_2Ge_2$ with $CaBe_2Ge_2$-type; complex magnetic order with ground state Eu^{2+}.**

INTRODUCTION

Our general interest in the magneto-electrical properties of ytterbium- and europium-containing compounds (1,2) and in particular of the corresponding silicides/germanides prompted us toward a closer inspection of the ternary systems Eu–Zn–Si and Eu–Zn–Ge. Due to the rather low melting and boiling point of europium metal ($T_m = 822°C$, $T_b = 1597°C$ (3)), synthesis of single-phase europium compounds with melting points higher than Eu is difficult to achieve via the usual high-frequency or arc-melting techniques. In recent papers (1,2) we demonstrated the use of an alternative technique for the growth of sizable single-crystal material based on the Lebeau method (4) employing low-melting flux solvents. The Lebeau technique was successfully used in the past with flux metals such as tin, copper, or aluminium to produce transition metal borides as well as silicides (5–7).

As a system internal flux, zinc metal was our first choice not only because of its low melting temperature but also for its good chemical interaction with europium and its readiness to dissolve the diluted HCl. Secondly, only few ternary silicides and germanides were reported so far with europium and zinc: hitherto only EuZnSi and EuZnGe, both with a ZrBeSi-type structure, are known as ternary compounds in the systems Eu–Zn–{Si, Ge} (8), and no further characterization of their physical properties has been reported. In a later stage of the project we also explored mixed flux systems such as Ga/Zn or In/Zn.

EXPERIMENTAL

The so-called Lebeau method (4) essentially depends on the temperature-dependent solubilities of Eu and Si(Ge) in the metal flux, which is contained in Al_2O_3 crucibles vacuum-sealed within thick-walled quartz tubes. The materials used were zinc granules, p.A. from Merck AG, D, 5 N gallium ingots from Alcan Electronics, CH, indium ingots, 99.9% pure, from Ögussa, A, 99.9% pure ingots of europium from Auer Remy, D, which were cut under cyclohexane to pieces smaller than 3 mm in size, and Si, Ge pieces, 99.99 mass%, from Alfa Ventron, D. A typical experiment started from room temperature with a heating rate of $75°C\ h^{-1}$ up to 875 to 1100°C with an intermediate hold at T_s of 400–450°C for 1 h above the melting point of the flux. After a soaking period at the top temperature for up to 24 h, cooling to 500–850°C proceeded at a speed of $25°C\ h^{-1}$, after which the sample batches were kept at this

[1] On leave from the Institute for Problems of Materials Science, Krzhyzhanovsky 3, Kiev, Ukraine.
[2] Present address: MPI-CPfS, D-01187 Dresden.
[3] To whom correspondence should be addressed. E-mail: peter.franz.rogl@univie.ac.at.

0022-4596/02 $35.00

temperature for 2–12 h prior to final quenching, when samples were simply removed from the hot furnace. Starting from various ratios [Eu + Si(Ge)]/flux, the heating and cooling rates were generally sufficient to produce good quality single-crystal specimens of the ternary europium–zinc–silicides (germanides). The single-crystal material was freed from the Zn metal by dissolving the matrix in 3 N HCl. Gallium- or indium-containing flux was usually removed in an ultrasonically agitated bath of mercury at room temperature. In some cases the flux was dissolved electrochemically: the flux was the anode against a $Hg/HgSO_4$ cathode (+ 900 mV, 65 mA/cm^2, 20°C). A 10^{-1} M K_2SO_4 solution served as an electrolyte. A detailed description of the experimental parameters used for the synthesis is given in Table 1 accompanying the crystallographic data listed.

Crystal identification was performed for a series of crystal specimens using a 57.3-mm radius Gandolfi camera, which also served for the determination of the unit cell dimensions. Precise lattice parameters and standard deviations were obtained by a least-squares refinement of room-temperature Guinier-Huber X-ray (Cu$K\alpha_1$) powder data from a set of crystals (optically selected under the microscope and powdered) employing an internal standard of 99.9999 mass% pure Ge or Si ($a_{Ge} = 0.5657906$, $a_{Si} = 0.5431065$ nm). Weissenberg photographs accomplished crystal quality control and inspection of crystal symmetry. Single-crystal X-ray intensity data for $EuZn_2Si_2$ ($EuZn_2Ge_2$) were collected for a hemisphere in 185 (284) images in a total exposure time of 61 min (176 min) on a four-circle Nonius Kappa diffractometer equipped with a CCD area detector employing graphite monochromatic Mo$K\alpha$ radiation ($\lambda = 0.071073$ nm). Orientation matrix and unit cell parameters were derived from the first ten data frames using the program DENZO (9). Absorption correction was taken from the program SORTAV (9) ($\mu_{EuZn_2Si_2} = 29.4$, $\mu_{EuZn_2Ge_2} = 41.8$ nm^{-1}). The structure was refined with the aid of the SHELXS-97 program (10).

The magnetic properties were studied in the temperature range 1.7–400 K and in magnetic fields up to 5 T employing a SQUID magnetometer (Quantum Design MPMS-5). The electrical resistivity was measured over the range 4.2–300 K by a conventional four-point dc technique on sufficiently large single-crystal specimens.

XAS was performed at the French synchrotron radiation facility (LURE) in Orsay using the X-ray beam of the DCI storage ring (working at 1.85 GeV and ~320 mA) on the EXAFS D21 station. A double Si(311) crystal was used as a monochromator. The rejection of third-order harmonics was achieved with the help of two parallel mirrors adjusted to cut off energies higher than ~10 keV. Experiments were carried out in the energy range 6900 to 7020 eV, which contains the L_{III}-edge of Eu. Finely powdered samples in cyclohexane were spread on an adhesive Kapton tape and four such tapes were stacked together for preparing a sample layer of thickness sufficient enough to ensure a good signal. Moreover, this was also helpful in eliminating, to a good extent, any sample-free regions in the path of the radiation. X-ray absorption spectra were measured at two fixed temperatures, 300 and 77 K for $EuZn_2Si_2$ and 300 and 10 K for the germanide.

RESULTS AND DISCUSSION

Crystal Structure of the Compounds $EuZn_2Si_2$ and $EuZn_2Ge_2$

To probe the potential of a suitable flux for the synthesis of ternary Zn-containing Eu–silicides and –germanides, several batches with different flux systems (pure Zn, 60%Ga + 40%Zn or 60%In + 40%Zn) were the subject of elaborate temperature programs (see Table 1). It is interesting to note that pure Zn flux was less efficient at producing high-quality and sizable single-crystal material. Whereas Zn-grown crystals generally were small and intergrown or twinned, Ga/Zn and In/Zn flux mixtures reproducibly resulted in good quality and large single crystals. Consequently, $EuZn_2Si_2$ was never obtained from Zn flux charges treated in 3 N HCl. The latter experiments yielded rather $EuZn_{13}$ than $EuZn_2Si_2$. This fact may be related to the sensitivity of $EuZn_2Ge_2$ and particularly of $EuZn_2Si_2$

TABLE 1
Crystallographic Data (Guinier) for the Ternary Europium Silicides and Germanides

Starting composition (molar ratio)	Temperature program for synthesis	Phase	Space group	Structure type	Lattice parameters (nm)	
					a	*c*
$(EuSi_2) + 4(In_3Zn_2)$	$T_{max}^{1100°C}$–$T_{min}^{600°C}$	$EuZn_2Si_2$	*I*4/*mmm*	$ThCr_2Si_2$	0.42587(7)	1.0383(3)
$(EuSi_2) + 4(Ga_3Zn_2)$	$T_{max}^{1100°C}$–$T_{min}^{600°C}$	$EuZn_2Si_2$	*I*4/*mmm*	$ThCr_2Si_2$	0.42610(7)	1.0397(4)
$(EuZn_2Si_2) + 50Zn$	$T_{max}^{875°C}$–$T_{min}^{500°C}$	$EuZn_{13}$	$Fm\bar{3}c$	$NaZn_{13}$	1.22128(8)	—
$(EuZn_2Ge_2) + 50Zn$	$T_{max}^{1050°C}$–$T_{min}^{850°C}$	$EuZn_2Ge_2$	*P*4/*nmm*	$CaBe_2Ge_2$	0.42852(7)	1.0801(3)
$(EuZn_2Ge_2) + 50Zn$	$T_{max}^{875°C}$–$T_{min}^{500°C}$	$EuZn_2Ge_2$	*P*4/*nmm*	$CaBe_2Ge_2$	0.4295(1)	1.0762(4)
$(EuSi_2) + 5(Ga_3Zn_2)$	$T_{max}^{1100°C}$–$T_{min}^{600°C}$	$EuZn_2Ge_2$	*P*4/*nmm*	$CaBe_2Ge_2$	0.43088(8)	1.0787(4)

against attach by the flux-dissolving acids. Although the various flux components yielded single-crystal material of widespread quality, unit cell dimensions were practically the same for each of the two compounds, confirming a negligible influence of the given flux on the stability of the product. Dissolution of the flux led to residues of in most cases (see also discussion above) rather well-shaped crystals (> 0.25 mm) with different growth habits (plates and

TABLE 2
Structure Refinement[a] for X-ray Single-Crystal Data of $EuZn_2Si_2$ ($ThCr_2Si_2$-Type) and $EuZn_2Ge_2$ with $CaBe_2Ge_2$-Type; Data Collected on Nonius Kappa CCD; Mo$K\alpha$

Parameter/compound	$EuZn_2Si_2$	$EuZn_2Ge_2$
Lattice parameters in (nm) refined from four-circle diffractometer	$a = 0.42607(2)$, $c = 1.03956(5)$	$a = 0.43095(2)$, $c = 1.07926(6)$
Space group; Z	$I4/mmm$, origin at -1, $Z = 2$	$P4/nmm$, origin at -1, $Z = 2$
Structure type	$ThCr_2Si_2$-type	$CaBe_2Ge_2$-type
Density, $\rho_{X\text{-ray}}$ in ($Mg\,m^{-3}$)	$\rho_{X\text{-ray}} = 5.96$	$\rho_{X\text{-ray}} = 7.09$
Data collection, 2θ range in degrees	2.0 to 80.5	2.0 to 90.6
Number of variables	8	15
Reflections in refinement	303 ($204 > 2\sigma$) (meas. 1549)	551 ($458 > 2\sigma$) (meas. 6374)
$R_{F^2} = \sum\|F_o^2 - F_c^2\|/\sum F_o^2$	0.038 ($I > 2\sigma$)	0.067 ($I > 2\sigma$)
$R_{wP} = [\sum w_i\|y_{oi} - y_{ci}\|^2/\sum w_i\|y_{oi}\|^2]^{1/2}$	$R_w = 0.104$	$R_w = 0.124$
$R_P = \sum\|y_{oi} - y_{ci}\|/\sum\|y_{oi}\|$	R_I(all data) = 0.038	R_I(all data) = 0.085
$R_e = \{(N - P + C)/(\sum w_i\|y_{oi}\|^2)\}^{1/2}$	Overall $R_{merge} = 0.096$	Overall $R_{merge} = 0.071$
$\chi^2 = (R_{wP}/R_e)^2$	GOF = 1.17	GOF = 1.30
Extinction (Zachariasen)	0.063(8)	0.043(4)
Atom parameters:		
	Eu in 2*a* (0, 0, 0)	**Eu in 2*c* ($\frac{1}{4}$, $\frac{1}{4}$, $z = 0.7495(1)$)**
$U_{eq.}(U_{iso})$ 10^2 (nm^2)	0.0053(3)[b]	0.0103(3)[c]
	Zn in *4d* ($0, \frac{1}{2}, \frac{1}{4}$)	**Zn1 in *2c* ($\frac{1}{4}$, $\frac{1}{4}$, $z = 0.1314(2)$)**
$U_{eq.}(U_{iso})$ 10^2 (nm^2)	0.0067(3)[b]	0.0130(5)[c]
	Si in *4e* (0, 0, $z = 0.3856(2)$)	**Zn2 in *2b* ($\frac{3}{4}$, $\frac{1}{4}$, $\frac{1}{2}$)**
U_{iso} 10^2 (nm^2)	0.0013(4)	0.0110(4)[c]
	—	**Ge1 in *2c* ($\frac{1}{4}$, $\frac{1}{4}$, $z = 0.3636(2)$)**
$U_{eq.}$ (U_{iso}) 10^2 (nm^2)		0.0072(4)[c]
	—	**Ge2 in *2a* ($\frac{3}{4}$, $\frac{1}{4}$, 0)**
$U_{eq.}$ (U_{iso}) 10^2 (nm^2)		0.0144(5)[c]

Interatomic distances < 4.5 nm						
Standard deviations < 0.00006 nm	**Eu**	8Si	0.32392	**Eu**	4Ge1	0.32827
		8Zn	0.33605		4Zn1	0.33075
		4Eu	0.42607		4Zn2	0.34484
					4Ge2	0.34576
	CN = 20			CN = 20	4Eu	0.43095
		—		**Zn1**	1Ge1	0.25068
					4Ge2	0.25794
				CN = 9	4Eu	0.33075
	Si	1Si	0.23793	**Ge1**	1Zn1	0.25068
		4Zn	0.25543		4Zn2	0.26093
	CN = 9	4Eu	0.32392	CN = 9	4Eu	0.32827
	Zn	4Si	0.25543	**Zn2**	4Ge1	0.26093
		4Zn	0.30128		4Zn2	0.30473
	CN = 12	4Eu	0.33605	CN = 12	4Eu	0.34484
		—		**Ge2**	4Zn1	0.25794
					4Ge2	0.30473
				CN = 12	4Eu	0.34576

[a]Crystal structure data were standardized using Program Structure Tidy (11).

[b]Anisotropic displacement factors (10^2 nm^2) are as follows: **Eu**, $U_{11} = U_{22} = 0.0045(3)$, $U_{33} = 0.0069(3)$, $U_{12} = U_{13} = U_{23} = 0$. **Zn**, $U_{11} = U_{22} = 0.0075(4)$, $U_{33} = 0.0050(4)$, $U_{12} = U_{13} = U_{23} = 0$.

[c]Anisotropic displacement factors (10^2 nm^2) are as follows: **Eu**, $U_{11} = U_{22} = 0.0088(3)$, $U_{33} = 0.0133(4)$, $U_{12} = U_{13} = U_{23} = 0$. **Zn1**, $U_{11} = U_{22} = 0.0122(6)$, $U_{33} = 0.0146(10)$, **Zn2**, $U_{11} = U_{22} = 0.0108(6)$, $U_{33} = 0.0115(7)$, **Ge1**, $U_{11} = U_{22} = 0.0094(5)$, $U_{33} = 0.0028(5)$, **Ge2**, $U_{11} = U_{22} = 0.0156(7)$, $U_{33} = 0.0118(7)$.

irregular forms). Inspection by Weissenberg and Gandolfi single-crystal X-ray diffractometry on suitable crystal fragments of several of the smaller crystal specimens revealed in most cases a mixture of Si(Ge) crystals with $EuZn_2M_2$ crystals in the shape of platelets. Weissenberg photographs gave no indication of superstructures or deviation from simple body-centered unit cells ($a = 0.43$ nm, $c = 1.03$ nm) for $EuZn_2Si_2$. Systematic extinctions, only observed for body centering, and unit cell dimensions suggested isotypism with the body-centered tetragonal $BaAl_4$-type of structure. Assuming an atomic arrangement corresponding to the $ThCr_2Si_2$-type (ordered variant of $BaAl_4$), model X-ray intensity calculations satisfactorily described the Gandolfi and Guinier X-ray diffraction patterns of the crystals. A close inspection of the heavily exposed Weissenberg films of $EuZn_2Ge_2$ revealed weak reflections with $h + k + l = 2n + 1$, giving evidence for a primitive unit cell. To clarify this and prove the assumed structural models, several crystals of $EuZn_2Ge_2$ and $EuZn_2Si_2$ were selected for automatic four-circle X-ray single-crystal diffractometry. Conditions of data collection and results of the structural refinements are given in Table 2. Occupancies have been refined, but no deviations from full occupation numbers could be detected. It should be mentioned that one of the anisotropic temperature factors, U_{33}, of Ge1 revealed strong correlations with the type of absorption correction and thus appears slightly smaller than the corresponding U_{11} values. Absorption correction essentially is responsible for the somewhat higher R values for the Ge-containing crystals (several crystals tried).

The structure of $EuZn_2Ge_2$ was found to fully correspond with the atomic arrangement of the $CaBe_2Ge_2$-type. As the X-ray scattering power of Zn ($Z = 30$) and Ge ($Z = 32$) differs only by two electrons, the distribution of Zn and Ge over the available atom sites in $P4/nmm$ could not be evaluated with certainty—in this case we followed the structural chemical analogs to isotypic ternary germanides. For the $EuZn_2Si_2$ crystal the structural refinement showed a completely ordered arrangement of four Zn atoms in the 4*d* sites and four Si atoms in the 4*e* sites of space group $I4/mmm$. Starting from the atomic arrangements for the $ThCr_2Si_2$-type ($EuZn_2Si_2$) and $CaBe_2Ge_2$-type ($EuZn_2Ge_2$), respectively (see i.e. Ref. (11)), both refinements converged without difficulties to residual values as low as 0.038 and 0.067, respectively. Results of the structural refinements are given in Table 2 including various residual values, anisotropic thermal parameters, and interatomic distances. A list of the intensity data may be obtained from the authors on request. The crystal structure of the compounds is characterized by layers of Eu atoms, sandwiched by infinite layers of interconnected tetragonal (Si, Ge)Zn_4 pyramids parallel to (001). For the stoichiometric compounds, Zn atoms are tetrahedrally surrounded by four Si, Ge atoms. Si and Ge have four Zn neighbors and one Ge, Si neighbor thus being tetragonal pyramidally coordinated (12). Si–Si distances in $EuZn_2Si_2$ and corresponding Ge1–Zn1 distances in $EuZn_2Ge_2$ are slightly shorter than the sum of atom radii, eventually indicating a tendency to form strongly bonded dumbbells.

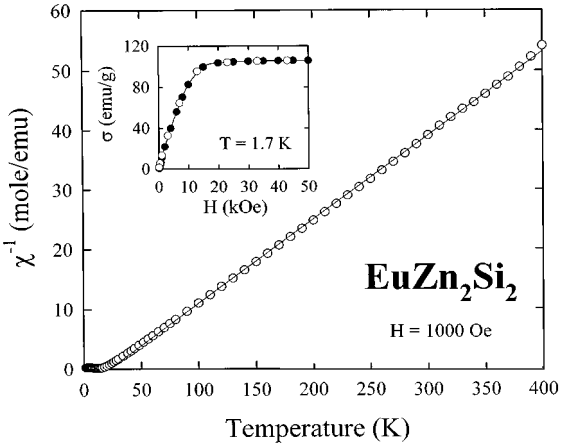

FIG. 1. Inverse molar magnetic susceptibility versus temperature for $EuZn_2Si_2$. The solid line is a Curie–Weiss fit with the parameters given in the text. Inset: Magnetization versus magnetic field strength for $EuZn_2Si_2$, taken at $T = 1.7$ K with increasing (full circles) and decreasing (open circles) field.

Magnetic and Electrical Properties

(*a*) *$EuZn_2Si_2$.* The magnetic behavior of $EuZn_2Si_2$ is shown in Fig. 1. Above ca. 50 K the magnetic susceptibility follows a Curie–Weiss law with the effective magnetic moment $\mu_{eff} = 7.54(5)\ \mu_B$ and the paramagnetic Curie temperature $\theta_p = 22(2)$ K. The experimental μ_{eff} is somewhat reduced with respect to the Russel–Saunders value expected for a free Eu^{2+} ion (7.94 μ_B). The relatively large positive θ_p may indicate the presence of strong ferromagnetic interactions. Indeed, as presented in the inset to Fig. 1, the magnetization of $EuZn_2Si_2$ exhibits at $T = 1.7$ K a field dependence characteristic of ferromagnetically ordered compounds. The $\sigma(H)$ curve saturates in magnetic fields stronger than 15 kOe, yielding a magnetic moment μ_s of 6.43(2) μ_B. Note that the latter value is rather close to the theoretical prediction for a free Eu^{2+} ion (6.76 μ_B).

A close inspection of the low-temperature magnetization of $EuZn_2Si_2$ measured in weak magnetic fields (see Fig. 2) upon cooling the sample in a zero (ZFC) and non-zero (FC) field gives evidence for very complex behavior in this compound. It orders magnetically at about 16 K, and this transition manifests itself only as a kink in $\sigma(T)$. Already at about 13 K (note the maximum in the $\sigma(T)$ variation) there occurs a subsequent phase transition, presumably a change in the spin structure. Both transitions have antiferromagnetic character as indicated by the absence of any splitting between the ZFC and FC magnetization curves above 11 K

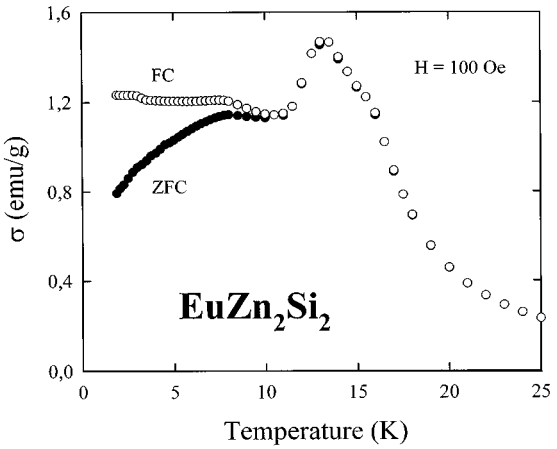

FIG. 2. Magnetization versus temperature (1.7–25 K) for $EuZn_2Si_2$. The data were measured at $H = 100$ Oe upon cooling the sample without (ZFC) and with (FC) an applied magnetic field.

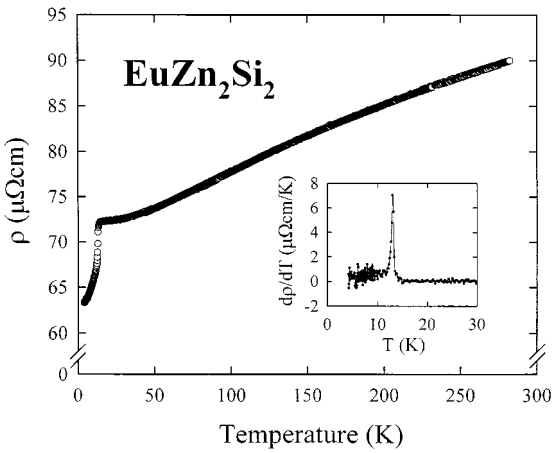

FIG. 4. Resistivity versus temperature for $EuZn_2Si_2$. Inset: Temperature derivative of the resistivity versus temperature (4.2–30 K) for $EuZn_2Si_2$.

(see Fig. 2) and featureless behavior of the imaginary component $\chi''(T)$ in the ac susceptibility (not shown). However, below ca. 11 K the magnetization of $EuZn_2Si_2$ does become sensitive to the magnetic history of the specimen and the $\chi''(T)$ susceptibility shows a peak. These two features hint to the development at lower temperatures of an uncompensated ferromagnetic component, likely due to some canting in the antiferromagnetic arrangement of the Eu magnetic moments. It seems that the canting angle $\alpha(T)$ increases with decreasing temperature and possibly the rate $d\alpha/dT$ undergoes two jumps at about 8 and 3.5 K, which result in kink-like anomalies on the $\sigma(T)$ curves (see Fig. 2).

In Fig. 3 is shown the field dependence of the magnetization of $EuZn_2Si_2$ measured at temperatures selected from the characteristic regions specified above. The $\sigma(B)$ curves taken at 1.9 and 5 K have a ferromagnetic-like character with saturation at nearly the same value. The magnetization measured at 12 and 15 K is almost proportional to the magnetic field strength in weak fields and shows a clear tendency to saturation in high fields. It is worth noting that the initial susceptibility at these temperatures is higher than that observed in the ferromagnetic-like region. Eventually, $\sigma(B)$ taken at 20 K is characteristic of short-range magnetic interactions in the paramagnetic region near the phase transition.

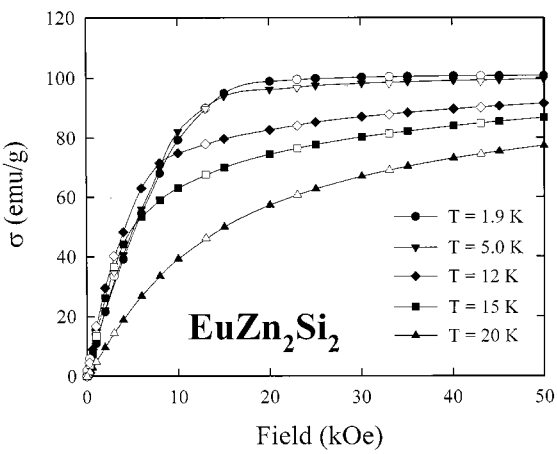

FIG. 3. Magnetization versus magnetic field strength for $EuZn_2Si_2$. The measurements were done at $T = 1.9$, 5.0, 12, 15, and 20 K with increasing (full symbols) and decreasing (open symbols) field.

The electrical resistivity of $EuZn_2Si_2$ has typical metallic character (see Fig. 4) with a room-temperature value of about 90 μΩ-cm. Below ca. 30 K, $\rho(T)$ shows a plateau at a relatively high value of 75 μΩ-cm and then drops rapidly. The pronounced kink in $\rho(T)$ leads to a very sharp maximum in the temperature derivative of the resistivity, which is displayed in the inset to Fig. 4. Interestingly, this distinct anomaly in the electrical properties occurs at $T = 13$ K, i.e., at the temperature where the magnetic susceptibility shows a major maximum and not at the Neel temperature $T_N = 16$ K (compare Fig. 2).

(*b*) *$EuZn_2Ge_2$*. As is apparent from Fig. 5, the inverse magnetic susceptibility of $EuZn_2Ge_2$ shows straight-line behavior at all temperatures above 20 K. The Curie–Weiss fit parameters are $\mu_{eff} = 7.89(3)\ \mu_B$ and $\theta_p = 10(2)$ K. The value of the effective magnetic moment is very close to the theoretical prediction for a free Eu^{2+} ion. The positive paramagnetic Curie temperature may suggest ferromagnetic-like properties at low temperatures, and this presumption seems justified by the $\sigma(H)$ variation taken at 1.7 K, which resembles very much that one measured for $EuZn_2Si_2$ (compare Fig. 1). The saturation magnetic moment amounts to 6.54(1) μ_B, which is close to the Russel–Saunders free ion value.

Yet the low-temperature magnetization of $EuZn_2Ge_2$ considerably differs from $\sigma(T)$ obtained for the silicide. As

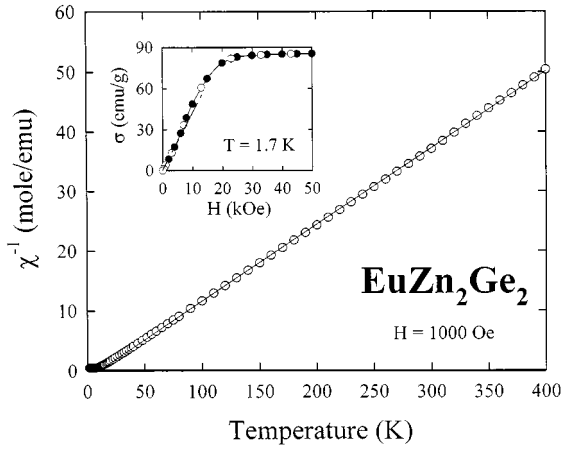

FIG. 5. Inverse molar magnetic susceptibility versus temperature for $EuZn_2Ge_2$. The solid line is a Curie–Weiss fit with the parameters given in the text. Inset: Magnetization versus magnetic field strength for $EuZn_2Ge_2$, taken at $T = 1.7$ K with increasing (full circles) and decreasing (open circles) field. The dashed line marks the region where σ is almost proportional to H.

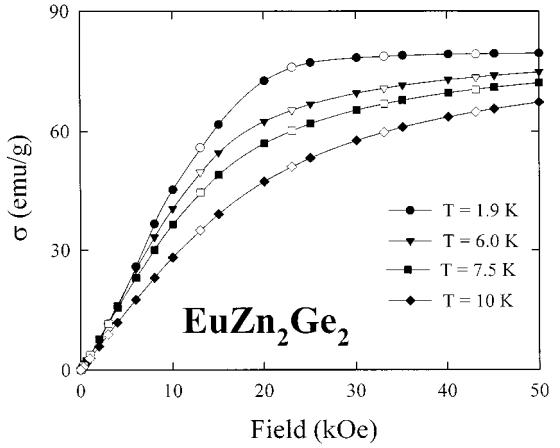

FIG. 7. Magnetization versus magnetic field strength for $EuZn_2Ge_2$. The measurements were done at $T = 1.9$, 6.0, 7.5, and 10 K with increasing (full symbols) and decreasing (open symbols) field.

displayed in Fig. 6, there occurs a kink in $\sigma(T)$ at 7.5 K, which probably signals an antiferromagnetic-like phase transition. Below this anomaly the magnetization diminishes only slightly with further decreasing temperature, with a little difference between the ZFC and FC curves. These findings suggest that the magnetic structure in $EuZn_2Ge_2$ has canted antiferromagnetic character.

The latter hypothesis seems corroborated by characteristic behavior of the field-dependent magnetization of $EuZn_2Ge_2$, taken at 1.7, 1.9, and 6 K (see the inset to Fig. 5 and Fig. 7), which exhibits metamagnetic-like anomalies in fields lower than about 5 kOe.

X-ray Absorption Spectroscopy

Eu L_{III}-edge spectra of $EuZn_2Si_2$ taken at 300 K and of $EuZn_2Ge_2$ at 10 K are shown in Fig. 8, with corresponding fitting curves (for clarity, curves have been shifted vertically). The larger peak at ≈ 6972 eV corresponds to the Eu^{2+} configuration and the smaller peak at ≈ 6980 eV corresponds to the Eu^{3+} configuration. The europium atoms are clearly in a nearly divalent state in the compounds, except for a minor trivalent contribution. Moreover, the relative weight of the two peaks does not vary with temperature from 300 to 10 K as shown in the inset of Fig. 8; i.e., the valence state is static and the minor contribution may correspond to a slight oxidation of the sample, e.g., when powdering it for X-ray absorption measurements.

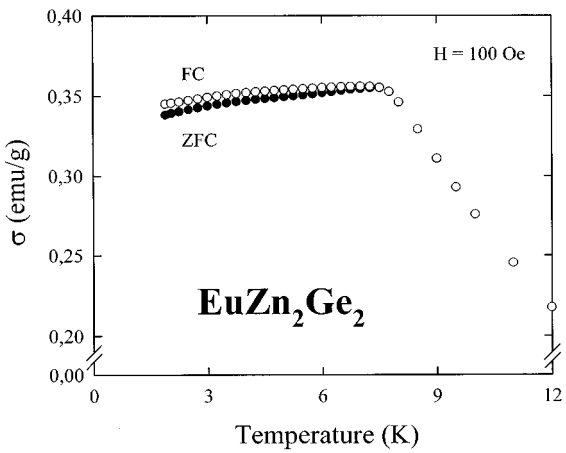

FIG. 6. Magnetization versus temperature (1.7–12 K) for $EuZn_2Ge_2$. The data were measured at $H = 100$ Oe upon cooling the sample without (ZFC) and with (FC) an applied magnetic field.

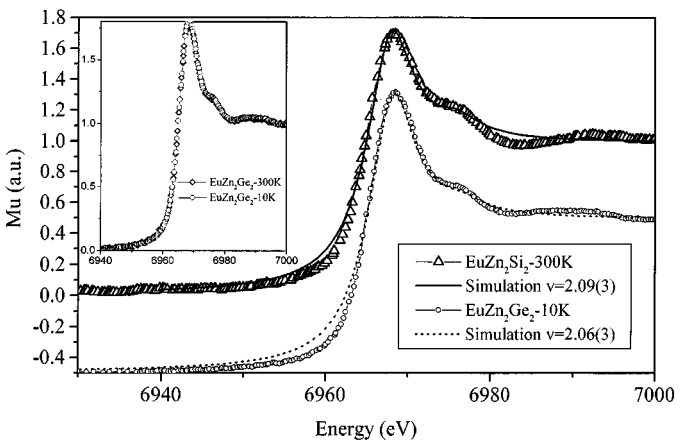

FIG. 8. X-ray absorption spectra of $EuZn_2Si_2$ at 300 K and of $EuZn_2Ge_2$ at 10 K. Lines correspond to respective simulation with values of valence v as given. For clarity, the curve for $EuZn_2Ge_2$ has been shifted vertically by -0.5 a.u.

With a classical technique (13), values of the valence $\langle v \rangle$ were found to be 2.06(3) at 300 and 10 K in $EuZn_2Ge_2$ and 2.09(3) at 300 and 77 K in $EuZn_2Si_2$. We must point out that this technique tests the valence of Eu ions, irrelevant of the fact that they belong to the matrix or to any impurity phase. It is clear that, for instance, a 6% ionic content of a trivalent Eu impurity would lead to this value of 2.06 if the matrix is divalent (i.e., 3% of Eu_2O_3 if oxide is formed when powdering).

ACKNOWLEDGMENTS

Thanks are due to Dr. A. Zaleski for the ac susceptibility measurements and Dr. G. Nauer of the Electrochemistry Department of the Institut für Physikalische Chemie for his kind advice in the electrochemical separation treatment. This research was supported by the Austrian FWF under Grant P9709. The authors (A. L.-J., D. K., and P. R.) are furthermore grateful to the OEAD and the Polish Academy of Sciences for support within the Austrian–Polish bilateral technical-scientific exchange programmes P13/99 and P14/01.

REFERENCES

1. B. Andraka, R. Petri, D. Kaczorowski, A.-Leithe-Jasper, and P. Rogl, *J. Appl. Phys.* **87,** 5149 (2000).
2. R. Petri, B. Andraka, and D. Kaczorowski, A.-Leithe-Jasper, and P. Rogl, *Phys. Rev. B* **61,** 12169 (2000).
3. "Binary Alloy Phase Diagrams" (T. B. Massalski, Ed.), 2nd ed. ASM, Materials Park, OH, 1990.
4. P. Lebeau and J. Figueras, *C. R. Acad. Sci. Paris* **136,** 1329 (1903).
5. D. Elwell and H. J. Scheel, "Crystal Growth from High-Temperature Solutions." Academic Press, London, 1975.
6. S. Okada, T. Atoda, I. Higashi, and Y. Takahashi, *J. Mater. Sci.* **22,** 2993 (1987).
7. Z. Fisk and J. P. Remeika, *in* "Handbook on the Physics and Chemistry of Rare Earths" (K. A. Gschneidner, Jr. and L. Eyring, Eds.), Vol. 12, p. 53. Elsevier Science, Amsterdam, 1989.
8. F. Merlo, M. Pani, and M. L. Fornasini, *J. Less-Common Met.* **171,** 329 (1991).
9. Nonius Kappa CCD Program Package COLLECT, DENZO, SCALEPACK, SORTAV, Nonius Delft, The Netherlands, 1998.
10. G. M. Sheldrick, SHELX-97, Program for Crystal Structure Refinement, University of Göttingen, Germany, 1997; Windows version by McArdle, Natl. Univ. Ireland, Galway.
11. E. Parthé, L. Gelato, B. Chabot, M. Penzo, K. Cenzual, and R. Gladyshevskii, "Typix-Standardized Data and Crystal Chemical Characterization of Inorganic Structure Types," Vol. 1, p. 233, Table E52; as a part of the "Gmelin Handbook of Inorganic and Organometallic Chemistry," 8th ed., Springer-Verlag, New York, 1994.
12. G. Just and P. Paufler, *J. Alloys Comp.* **232,** 1 (1996).
13. C. Godart, H. Flandorfer, and P. Rogl, *Physica B* **199–200,** 512 (1994).